A SECOND ORDER TURBULENCE MODEL BASED ON A REYNOLDS STRESS APPROACH FOR TWO-PHASE BOILING FLOW AND APPLICATION TO FUEL ASSEMBLY ANALYSIS

S. Mimouni [1] , F. Archambeau[1], M. Boucker[1], J. Lavieville[1,]

C. Morel[2]

stephane.mimouni@edf.fr,

(*1) Electricité de France R&D Division, 6 Quai Watier F-78400 Chatou, France,*

(2) Commissariat à l'Energie Atomique, 17 rue des Martyrs, F-38000 Grenoble, France

Abstract

High-thermal performance PWR (pressurized water reactor) spacer grids require both low pressure loss and high critical heat flux (CHF) properties. Numerical investigations on the effect of angles and position of mixing vanes and to understand in more details the main physical phenomena (wall boiling, entrainment of bubbles in the wakes, recondensation) are required.
In the field of fuel assembly analysis or design by means of CFD codes, the overwhelming majority of the studies are carried out using two-equation Eddy Viscosity Models (EVM), especially the standard $K-\varepsilon$ model, while the use of Reynolds Stress Transport Models (RSTM) remain exceptional.

But extensive testing and application over the past three decades have revealed a number of shortcomings and deficiencies in Eddy Viscosity Models. In fact, the $K-\varepsilon$ model is totally blind to rotation effects and the swirling flows can be regarded as a special case of fluid rotation. This aspect is crucial for the simulation of a hot channel in a fuel assembly. In fact, the mixing vanes of the spacer grids generate a swirl in the coolant water, to enhance the heat transfer from the rods to the coolant in the hot channels and to limit boiling.

First, we started to evaluate computational fluid dynamics results against the AGATE-mixing experiment: single-phase liquid water tests, with Laser-Doppler liquid velocity measurements upstream and downstream of mixing blades. The comparison of computed and experimental azimuthal (circular component in a horizontal plane) liquid velocity downstream of a mixing vane for the AGATE-mixing test shows that the rotating flow is qualitatively well reproduced by NEPTUNE_CFD but azimuthal liquid velocity is underestimated with the $K-\varepsilon$ model.

Before comparing performance of EVM and RSTM models, we seek to apply the Best Practice Guidelines[1] (BPG) to quantify the numerical errors. Due to the geometry and mesh size of cases featuring spacer grids, only few sensitivity tests can be performed. Therefore, we applied some recommendations of the BPG to two cases with very similar conditions but with a simpler geometry, the DEBORA-tube case and the ASU-annular channel case.

Then, a geometry closer to actual fuel assemblies is considered. It consists of a rectangular test section in which a 2x2 rod bundle equipped with a simple spacer grid with mixing vanes is inserted. The influence of the turbulence model on target variables linked to CHF limitation will be discussed. Moreover, the sensitivity to the mesh refinement will be particularly examined. The study of this case is a further step towards the modelling of the two-phase boiling flow in real-life grids and rod bundles.

1 NOMENCLATURE

A_i interfacial area concentration

[1] Best Practice Guidelines for the use of CFD in Nuclear Reactor Safety Applications, NEA/CSNI/R(2007)5

C_d drag coefficient
Δt numerical time step
$\underline{g}$ gravity acceleration
K_l liquid turbulent kinetic energy
$\underline{M}_k$ interfacial momentum transfer per unit volume and unit time
p pressure
Pr_l liquid Prandtl number
$\underline{\underline{R}}_k$ Reynolds stress tensor.
Re_b bubble Reynolds number
t time
u'_i fluctuation of the liquid velocity
$\underline{V}_k$ averaged velocity of phase k
$\underline{V}_{ki}$ interfacial-averaged velocity
α_k, denotes the time fraction of phase k
ε_l dissipation rate
μ_g gas molecular viscosity
ν_l liquid kinematic viscosity
ν_l^T liquid turbulent eddy viscosity
ρ_k, averaged density of phase k
σ surface tension
τ_w wall shear stress
$\underline{\underline{\Sigma}}_k$ molecular stress tensor

Subscripts/Superscripts
l liquid state
v vapour bubbles
k phase $k = l$ or v

2 INTRODUCTION

In a Pressurized Water nuclear Reactor, an optimum heat removal from the surface of the nuclear fuel elements (rod bundle with spacer grids) is very important for thermal margins and safety.

The geometry of the fuel assembly spacer grids has a strong influence on the safety and performance issues, in particular the grid vanes inclination angle. In (Shin, 2005), the Critical Heat Flux (CHF) experiment on the effect of the angle and of the position of mixing vanes was performed in a 2x2 rod bundle. The authors show that the mixing vanes increase the value of the CHF and the result is correlated to the magnitude of the swirl generated by the mixing vanes. If the angle of the mixing vanes is relatively small, the magnitude of the swirling flow is smaller because the rotating force created by the mixing vanes is weak. If the angle of the mixing vanes is relatively large, the mixing vanes play the role of flow obstacle under the Departure from Nucleate Boiling (DNB) condition. Therefore, it is important that the turbulence modelling deal with rotation effects.

There have been several studies on flow mixing and heat transfer enhancement caused by a mixing-vane spacer grid in a rod bundle geometry. Lee et al. (Lee, 2007) simulate the flow field and heat transfer in a

single phase flow for a 17x17 rod bundle with eight spans of mixing vanes. The FLUENT commercial code is employed and a Reynolds Stress Transport Model (RSTM) is used for turbulence. According to the authors, RSTM is helpful. Ikeda et al. (Ikeda, 2006) study an assembly consisting of a 5x5 heater rod bundle and eight specific mixing vane grids. For Ikeda et al., it might be insufficient to apply a standard $K-\varepsilon$ model to swirl-mixing flow and narrow-channel flow conditions that include non-isotropic effects. Moreover, In et al. (In, 2008) have performed a series of CFD single phase flow simulations to analyse the heat transfer enhancement in a fully heated rod bundle with mixing-vane spacers. For future work, In et al. recommend that a refined Computational Fluid Dynamic (CFD) model be developed to include details of the grid structure and a higher-order turbulence model be employed to improve the accuracy of such simulations.

Additional two-phase effects like accumulation of bubbles in the centre of sub-channel or pockets of bubbles on the rods should be taken into account to improve the simulation of flow close to DNB. Indeed, single-phase simulations remain insufficient and boiling flows simulations are required. In (Krepper, 2007), the authors describe CFD approaches to subcooled boiling and investigate their capability to contribute to fuel assembly design. A large part of their work is dedicated to the modelling of boiling flows and to forces acting on the bubbles. The authors note that the size of bubbles in the bulk is correlated to the local subcooling which is an important parameter (see (Shin, 2005)).

Considering flow in a PWR core in conditions close to nominal, when boiling occurs, a high velocity steady flow takes place with very small times scales associated to the passage of bubbles (10^{-4} s – 10^{-3} s) and with quite small bubble diameters (10^{-5} to 10^{-3} m) compared to the hydraulic diameter (about 10^{-2} m). According to the synthesis of the work performed in WP2.2 of the NURESIM project (Bestion, 2007), these are perfect conditions to use a time average or ensemble average of equations as usually done in the RANS approach. All turbulent fluctuations and two-phase intermittency scales can be filtered since they are significantly smaller than the scales of the mean flow.

The Large Eddy Simulation is also a possible approach. In the context of the NURESIM project, several studies have been carried out with a Large Eddy Simulation to study the axial development of air-water bubbly flows in a pipe. But in the synthesis of the work performed in WP2.2, it is noted in (Bestion, 2007) that several open modelling and numerical issues still remain. So, we will focus on the RANS approach in this paper.

According to all these recommendations, a better understanding of the detailed structure of a flow mixing and heat transfer downstream of a mixing-vane spacer in a nuclear fuel rod bundle has to be investigated with a RSTM.

Moreover, the overwhelming majority of industrial CFD applications today are still conducted with two-equation eddy viscosity model, especially the standard $K-\varepsilon$ model, while RSTM remain exceptional.

As an example of RSTM development, a RSTM model adapted to bubbly flows is studied in (Chahed, 1999) and used to perform simulations of three basic bubbly flows (grid, uniform shear and bubbly wake). The authors decomposed the Reynolds stress tensor of the liquid into two independent parts: a turbulent part produced by the mean velocity gradient that also contains the turbulence of the bubble wakes and a pseudo-turbulent part induced by bubble displacements; each part is predicted from a transport equation. This model is interesting but has not been selected here for the following reasons. Firstly, the computation effort is doubled (turbulent and pseudo-turbulent parts). Secondly, considering the flow close to nominal PWR core conditions, when boiling occurs, a high velocity steady flow takes place and the bubble diameter is quite small (10^{-5} to 10^{-3} m): therefore, the bubbles follow the liquid streamlines and so the modelling of the pseudo-turbulent part induced by bubble displacements can be omitted. Thirdly, the two-phase flow modelling proposed in (Chahed, 1999) does not tend to a single-phase flow formulation when the void fraction tends to zero. These three arguments have imposed the choice of the higher-order turbulence model described in the paper.

A second-order moment turbulence model for simulating a bubble column is also proposed in (Zhou, 2002). The authors defined a Reynolds tensor for each phase. Furthermore, following a similar method used in deriving and closing the Reynolds stress equations, a modelled transport equation of two-phase fluctuating velocity correlations is also solved. For the same reasons as those mentioned above for the model proposed in (Chahed, 1999), we have not adopted the model proposed in (Zhou, 2002). The turbulence modelling described in the present paper takes into account the Reynolds tensor for the liquid only, while a more basic modelling is used for the vapour phase.

However, to the authors' knowledge, no industrial CFD approach for boiling flows with a RSTM approach is available in the context of the fuel assembly design. This may be due to the fact that numerical problems may occur when using a RSTM approach without caution. Furthermore, the turbulence modelling of boiling flows is not straightforward. The use of RSTM also requires finer meshes than eddy viscosity models (EVM) and RSTM may therefore be more time and storage consuming. Developing an industrial RSTM approach is a quite challenging task but it is worth working at it: RSTM and EVM results will probably differ and it is important to determine what consequences it may have on thermal margin and safety of reactors.

In the framework of a R&D programme carried out in the NEPTUNE project (EDF, CEA, AREVA-NP, IRSN), the following strategy has been adopted:

1. validation of the NEPTUNE_CFD code with a RSTM approach on single phase flow with mixing vanes and on more academic cases of air-water adiabatic bubbly flows in a pipe;
2. validation of the NEPTUNE_CFD code with a RSTM approach on boiling flows in a pipe and sensitivity to the angle of the vanes for fuel assembly spacer grids performed in a 2x2 rod bundle in a boiling flow configuration;
3. validation of the NEPTUNE_CFD code with a RSTM approach for a 5x5 rod bundle with mixing vanes currently used for commercial nuclear fuel.

The step 1 is described in (Mimouni, 2008b). The second step is developed in the present paper. The step 3 is not yet started. Our main objective in this paper is to check that the simulation with the RSTM gives satisfactory results in a simple geometry as compared to a EVM: this point is crucial before calculating rod bundle geometries where the EVM model may fail.

This paper is organized as follows. In section 3 the general model we use for two-phase boiling flow simulations is presented in detail. In section 4, we underline the weaknesses of the EVM models. In section 6, the second-moment closure model for high Reynolds number two-phase flows is presented. In sections 7 and 8 respectively, the DEBORA case and the ASU case are briefly described. The comparison of the results of NEPTUNE_CFD calculations and the experimental data are presented. The sensitivity of the numerical results to the turbulence model for the fluid and to the most important models is studied. The section 9 is dedicated to calculations of geometry close to actual fuel assemblies in PWR conditions.

Finally, conclusions are drawn about our current capabilities to simulate boiling flows with a RSTM model and perspectives for future work are given.

3 THE NEPTUNE_CFD SOLVER AND PHYSICAL MODELLING

3.1 Introduction

NEPTUNE_CFD is a three dimensional two-fluid code developed more especially for nuclear reactor applications. This local three-dimensional module is based on the classical two-fluid one pressure approach, including mass, momentum and energy balances for each phase.

The NEPTUNE_CFD solver, based on a pressure correction approach, is able to simulate multi-component multiphase flows by solving a set of three balance equations for each field (fluid component

and/or phase) (Guelfi, 2007), (Mimouni, 2006, 2008, 2008b). These fields can represent many kinds of multiphase flows: distinct physical components (e.g. gas, liquid and solid particles); thermodynamic phases of the same component (e.g.: liquid water and its vapour); distinct physical components, some of which split into different groups (e.g.: water and several groups of different diameter bubbles); different forms of the same physical components (e.g.: a continuous liquid field, a dispersed liquid field, a continuous vapour field, a dispersed vapour field). The solver is based on a finite volume discretization, together with a collocated arrangement for all variables. The data structure is totally face-based, which allows the use of arbitrary shaped cells (tetraedra, hexahedra, prisms, pyramids ...) including non conforming meshes (meshes with hanging nodes).

3.2 Governing equations and physical modelling

The CFD module of the NEPTUNE software platform is based on the two-fluid approach (Ishii, 1975), (Delhaye, 1981). In this approach, a set of local balance equations for mass, momentum and energy is written for each phase. These balance equations are obtained by ensemble averaging of the local instantaneous balance equations written for the two phases. When the averaging operation is performed, the major part of the information about the interfacial configuration and the microphysics governing the different types of exchanges is lost. As a consequence, a number of closure relations (also called constitutive relations) must be supplied for the total number of equations (the balance equations and the closure relations) to be equal to the number of unknown fields. We can distinguish three different types of closure relations: those which express the inter-phase exchanges (interfacial transfer terms), those which express the intra-phase exchanges (molecular and turbulent transfer terms) and those which express the interactions between each phase and the walls (wall transfer terms). The balance equations of the two-fluid model we use for two-phase boiling flows and their closure relations are described in the following subsections.

3.2.1 Main set of balance equations

The two-fluid model we use for our two-phase boiling flow calculations consists of the following balance equations.

Two mass balance equations:

$$\frac{\partial \alpha_k \rho_k}{\partial t} + \nabla.\left(\alpha_k \rho_k \underline{V}_k\right) = \Gamma_k \qquad k = l, v \tag{1}$$

where t is the time, α_k, ρ_k, $\underline{V}_k$ denote the time fraction of phase k, its averaged density and velocity. The phase index k takes the values l for the liquid phase and v for vapour bubbles.

Two momentum balance equations:

$$\frac{\partial \alpha_k \rho_k \underline{V}_k}{\partial t} + \nabla.\left(\alpha_k \rho_k \underline{V}_k \underline{V}_k\right) = -\alpha_k \underline{\nabla} p + \underline{M}_k + \alpha_k \rho_k \underline{g} + \nabla.\left[\alpha_k \left(\underline{\underline{\Sigma}}_k + \underline{\underline{R}}_k\right)\right] \qquad k = l, v, \tag{2}$$

where p is the pressure, $\underline{g}$ is the gravity acceleration, $\underline{M}_k$ is the interfacial momentum transfer per unit volume and unit time, and $\underline{\underline{\Sigma}}_k$ and $\underline{\underline{R}}_k$ denote the molecular and turbulent stress tensors, the latter being also called the Reynolds stress tensor. The wall friction terms for the two phases do not appear in the momentum balance equations because solid walls are only present at the boundaries of the flow domain and the wall friction is expressed through the wall boundary conditions.

Two total enthalpy balance equations:

$$\frac{\partial}{\partial t}\left[\alpha_k \rho_k \left(h_k + \frac{V_k^{\,2}}{2}\right)\right] + \nabla.\left(\alpha_k \rho_k \left(h_k + \frac{V_k^{\,2}}{2}\right)\underline{V}_k\right) = \alpha_k \frac{\partial p}{\partial t} + \alpha_k \rho_k \underline{g}.\underline{V}_k + \Gamma_k \left(h_{ki} + \frac{V_k^{\,2}}{2}\right) \tag{3}$$
$$+ \Pi'_k A_i + q'''_{wk} - \nabla.\left[\alpha_k \left(\underline{q}_k + \underline{q}_k^{\,T}\right)\right] \qquad k = l, v$$

where h_k is the phase-averaged enthalpy for phase k and h_{ki} is the interfacial-averaged enthalpy. We have assumed that the two phases are governed by the same averaged pressure field p and we make no

distinction between the pressures in the two phases or between the bulk pressure and the interface pressure for simplicity. The three terms Γ_k, $\underline{M}_k$ and $\Pi'_k A_i$ denote the interfacial transfer terms of mass, momentum and heat, the quantity A_i being the interfacial area concentration. The terms q'''_{wk} denote the wall-to-fluid heat transfer per unit volume and unit time for each phase. The two terms $\underline{q}_k$ and $\underline{q}_k^T$ denote the molecular and turbulent heat fluxes inside phase *k*.

The interfacial transfer of momentum $\underline{M}_k$ appearing in the RHS of Eq. (2) is assumed to be the sum of four forces:

$$\underline{M}_k = \underline{M}_k^D + \underline{M}_k^{AM} + \underline{M}_k^L + \underline{M}_k^{TD} \tag{4}$$

The four terms are the averaged drag, added mass, lift and turbulent dispersion forces per unit volume. Now we will give the expressions we use for these forces and for their coefficients.

- Drag force:

$$\underline{M}_v^D = -\underline{M}_l^D = -\frac{1}{8} A_i \rho_l C_D \left|\underline{V}_v - \underline{V}_l\right| \left(\underline{V}_v - \underline{V}_l\right), \tag{5}$$

where C_D is the drag coefficient for bubbles and can be determined experimentally.

- Added-mass force:

$$\underline{M}_v^{AM} = -\underline{M}_l^{AM} = -C_A^{lv} \frac{1+2\alpha_v}{1-\alpha_v} \alpha_v \rho_l \left[\left(\frac{\partial \underline{V}_v}{\partial t} + \underline{V}_v . \underline{\underline{\nabla}} \underline{V}_v \right) - \left(\frac{\partial \underline{V}_l}{\partial t} + \underline{V}_l . \underline{\underline{\nabla}} \underline{V}_l \right) \right], \tag{6}$$

where C_A^{lv} is the added mass coefficient which is equal to ½ for a spherical bubble and the factor $(1+2\alpha)/(1-\alpha)$ takes into account the effect of the bubbles concentration (Zuber, 1964), (Ishii, 1990).

- Lift force:

$$\underline{M}_v^L = -\underline{M}_l^L = -C_L \alpha_v \rho_l \left(\underline{V}_v - \underline{V}_l\right) \wedge \left(\underline{\nabla} \wedge \underline{V}_l\right), \tag{7}$$

where C_L is the lift coefficient. This coefficient is equal to ½ in the particular case of a weakly rotational flow around a spherical bubble in the limit of infinite Reynolds number (Auton, 1987).

- Turbulent dispersion force:

$$\underline{M}_v^{TD} = -\underline{M}_l^{TD} = -C_{TD} \rho_l K_l \underline{\nabla} \alpha_v, \tag{8}$$

where K_l is the liquid turbulent kinetic energy and C_{TD} is a numerical constant of order 1. This expression was proposed by Lance (Lance, 1994).

An alternative approach is proposed by (Deutsch, 1991) to model the turbulence induced by bubbles: an algebraic model developed in the framework of Tchen's theory where the turbulent kinetic energy for the dispersed phase and the covariance are calculated from the turbulent kinetic energy of the continuous phase.

For the dispersed phase, the Reynolds stress tensor is closed using a Boussinesq-like hypothesis:

$$\underline{\underline{R}}_v = \rho_v \nu_v^T \left(\underline{\underline{\nabla}} \underline{V}_v + \underline{\underline{\nabla}}^T \underline{V}_v\right) - \frac{2}{3} \underline{\underline{I}} \left(\rho_v K_v + \rho_v \nu_v^T \nabla . \underline{V}_v\right) \tag{9}$$

where $\underline{\underline{I}}$ is the identity tensor,

with: $\nu_v^T = \frac{1}{3} q_{lv} \left(\tau_{lv}^t - \frac{C_A^{lv} \tau_{lv}^F}{\frac{\rho_v}{\rho_l} + C_A^{lv}} \frac{\tau_{lv}^F}{2} \right) + \frac{1}{3} K_v \tau_{lv}^F$, the turbulent viscosity for the dispersed phase,

$K_v = K_l \left(\frac{b^2 + \eta_r}{1 + \eta_r} \right)$, the gas turbulent kinetic energy,

$q_{lv} = K_l \left(\frac{b + \eta_r}{1 + \eta_r} \right)$, the covariance of the dispersed phase,

$b = \frac{1 + C_A^{lv}}{\frac{\rho_v}{\rho_l} + C_A^{lv}}$

$\eta_r = \frac{\tau_{lv}^t}{\tau_{lv}^F}$, the ratio between the time scale of the continuous phase turbulence seen by the dispersed phase (that takes into account crossing trajectories effect) and the characteristic time scale of the momentum transfer rate between the liquid and dispersed phases:

$\tau_{lv}^t = \frac{\tau_l^t}{\sigma_\alpha} \left(1 + C_\beta \xi_r^2 \right)^{-\frac{1}{2}}$ with σ_α is the turbulent Schmidt or Prandtl turbulent for the continuous phase, C_β is the crossing trajectories coefficient taken equal to 1.8, C_A^{lv} is the added mass coefficient,

$\tau_{lv}^F = \frac{C_A^{lv} + \rho_v}{F_D^{lv}}$

with $\xi_r = \frac{\langle \left| \overrightarrow{V_r} \right| \rangle_v}{\sqrt{\frac{1}{3} k_l}}$ and $\tau_l^t = \frac{3}{2} C_\mu \frac{K_l}{\varepsilon_l}$.

It can be shown that the turbulent dispersion force is a particular case of the Tchen's theory where C_{TD} is a function of the physical quantities defined above and does not need any parameters.

For the sake of simplicity, the turbulent dispersion force is used in the DEBORA tests and ASU tests, but the Tchen's theory is used in the industrial geometry studied in the paper and in (Mimouni, 2008, 2008b).

3.2.2 Turbulent transfer terms

The $K - \varepsilon$ model describes energy processes in terms of production and dissipation, as well as transport through the mean flow or by turbulent diffusion. The Kolmogorov spectral equilibrium hypothesis also enables one to predict a large eddy length-scale. On the other hand, the anisotropy of the stresses is quite crudely modelled. First of all the EVM model assumes the Reynolds stress tensor is aligned with the strain rate tensor (Boussinesq approximation):

$$\underline{\underline{R}}_l = \rho_l \nu_l^T (\underline{\underline{\nabla}} \underline{V}_l + \underline{\underline{\nabla}}^T \underline{V}_l) - \frac{2}{3} \underline{\underline{I}} (\rho_l K_l + \rho_l \nu_l^T \nabla . \underline{V}_l) , \quad (10)$$

where $\underline{\underline{I}}$ is the identity tensor, K_l is the liquid turbulent kinetic energy and ν_l^T is the liquid turbulent eddy viscosity. The liquid turbulent eddy viscosity is expressed by the following relation:

$$\nu_l^T = C_\mu \frac{K_l^2}{\varepsilon_l} , \quad (11)$$

where $C_\mu = 0.09$. The turbulent kinetic energy K_l and its dissipation rate ε_l are calculated by using the two-equations $K-\varepsilon$ approach.

3.2.3 Interfacial transfer terms

If the mechanical terms are neglected in comparison to the thermal terms in the averaged form of the energy jump condition, this condition reduces to:

$$\sum_k \left(\Gamma_k h_{ki} + q''_{ki} A_i\right) \approx 0 . \tag{12}$$

This important relation (together with the mass jump condition $\Gamma_l = -\Gamma$) allows to compute the mass transfer terms as functions of the interfacial heat transfer terms $q''_{ki} A_i$ and the interfacial-averaged enthalpies h_{ki} :

$$\Gamma_l = -\Gamma_v = \frac{q''_{li} + q''_{vi}}{h_{vi} - h_{li}} A_i . \tag{13}$$

We have no information about the dependence of the interfacial- averaged enthalpies h_{ki}. Therefore, two basic assumptions can be made: (1) the interfacial-averaged enthalpies h_{ki} are identified to the phase-averaged ones h_k or (2) the interfacial-averaged enthalpies h_{ki} are given by the saturation enthalpies. Here we have made the assumption (1). Each interfacial heat transfer term $q''_{ki} A_i$ is the product of the interfacial heat flux density:

$$q''_{ki} = C_{ki}\left(T_{sat}(p) - T_k\right), \tag{14}$$

where C_{ki}, T_k and $T_{sat}(p)$ denote a heat transfer coefficient, the averaged temperature of phase k and the saturation temperature. The interfacial area concentration is expressed as $A_i = 6\alpha / d$, where α is the void fraction and d is the mean bubble diameter. The following heat transfer coefficient is used:

$$C_{li} = \frac{Nu_l k_l}{d} \quad Nu_l = 2 + 0.6\,\mathrm{Re}^{1/2}\,\mathrm{Pr}_l^{1/3} \quad \mathrm{Re}_b \triangleq \frac{\left|\underline{V}_v - \underline{V}_l\right| d}{\nu_l} \quad \mathrm{Pr}_l \triangleq \frac{\nu_l}{a_l}, \tag{15}$$

where Re_b is the bubble Reynolds number and Pr_l is the liquid Prandtl number, ν_l being the liquid kinematic viscosity. The heat transfer coefficient between the vapour and the interface for the case of bubbles is written as:

$$C_{vi} A_i = \frac{\alpha \rho_v C_{pv}}{t_c}, \tag{16}$$

where C_{pv} is the gas heat capacity at constant pressure and t_c is a characteristic time given by the users. This relation simply ensures that the vapour temperature T_v remains very close to the saturation temperature T_{sat}, which is the expected result for bubbly flows with sufficiently small bubbles (flow in a PWR core in conditions close to nominal).

3.2.4 Wall transfer model for nucleate boiling

In a first simplified approach, and following the analysis of Kurul (Kurul, 1990), the boiling heat flux is split into three terms:

- a single phase flow convective heat flux q_c at the fraction of the wall area unaffected by the presence of bubbles,
- a quenching heat flux q_q where bubbles departure bring cold water in contact with the wall periodically,
- a vaporisation heat flux q_e needed to generate the vapour phase.

Each of these three phenomena is expressed by a heat flux density (per unit surface of the heated wall) which is related to the volumetric heat flux by the following relation:

$$q'''_{wl} = \frac{A_w}{V} q''_{wl} = \frac{A_w}{V}\left(q_c + q_q + q_e\right), \tag{17}$$

where A_w is the heated wall surface in contact to the cell having volume V, therefore q'''_{wl} is expressed in W/m^3 and q''_{wl} as well as q_c, q_q and q_e are expressed in W/m^2. The quantities q_c, q_q and q_e denote the heat flux densities due to liquid convective heat transfer, quenching and evaporation respectively. The liquid convective heat transfer per unit surface of the heated wall is written as:

$$q_c = A_c h_{\log}\left(T_w - T_l\right), \tag{18}$$

where T_w is the wall temperature and h_{log} is a heat exchange coefficient which is given by:

$$h_{\log} = \rho_l C_{pl} \frac{u^*}{T^+}, \tag{19}$$

where u^* is the wall friction velocity and T^+ is the non-dimensional liquid temperature. The velocity u^* is calculated from the logarithmic law of the wall written for the liquid velocity in the wall boundary layer. The non-dimensional temperature follows a similar logarithmic profile.

The heat flux density due to quenching is written as:

$$q_q = A_b t_q f \frac{2\lambda_l\left(T_w - T_l\right)}{\sqrt{\pi a_l t_q}}, \tag{20}$$

where A_b is the wall fraction occupied by bubble nucleation, f is the bubble detachment frequency, t_q is the quenching time and a_l is the liquid thermal diffusivity. The two fractions A_c and A_b are given by:

$$\begin{aligned} \mathrm{A_b} &= \min\left(1, \mathrm{n}\pi \mathrm{d_d}^2/4\right) \\ \mathrm{A_c} &= 1 - \mathrm{A_b} \end{aligned}, \tag{21}$$

where n is the active nucleation sites density (per unit surface of the heated wall) and d_d is the bubble detachment diameter. The active nucleation sites density is modelled according to (Kurul, 1990):

$$n = \left[210\left(T_w - T_{sat}\right)\right]^{1.8}, \tag{22}$$

as a function of the wall superheating. The bubble detachment diameter is given by the correlation from Unal (Unal, 1977). The Unal's correlation is valid for subcooled liquid but has been extended to saturated liquid. The bubble detachment diameter is given by:

$$d_d = 2.4210^{-5}\, p^{0.709} \frac{a}{\sqrt{b\varphi}}, \tag{23}$$

where p is the pressure and a, b and φ are given by the following relations:

$$a = \frac{\left(T_w - T_{sat}\right)\lambda_s}{2\rho_v \ell \sqrt{\pi a_s}}, \tag{24}$$

where λ_s and a_s denote the wall conductivity and thermal diffusivity, ρ_v denotes the vapour density and ℓ is the latent heat of vaporisation. In the modified correlation, b is given by:

$$b = \begin{cases} \dfrac{\left(T_{sat} - T_l\right)}{2\left(1 - \rho_v/\rho_l\right)} & St < 0.0065 \\ \dfrac{1}{2\left(1-\rho_v/\rho_l\right)} \dfrac{q_c + q_q + q_e}{0.0065 \rho_l C_{pl} \left\|V_l\right\|} & St > 0.0065 \end{cases}, \tag{25}$$

where $\left\|V_l\right\|$ is the norm of the liquid velocity and St is the Stanton number which is defined by:

$$St \triangleq \frac{q_c + q_q + q_e}{\rho_l C_{pl} \left\|V_l\right\| \left(T_{sat} - T_l\right)}, \tag{26}$$

and the quantity φ appearing in Eq. (23) is given by :

$$\varphi = \max\left(1, \left(\frac{\|V_l\|}{V_0}\right)^{0.47}\right) \qquad V_0 = 0.61 m/s, \tag{27}$$

The quenching time and the bubble detachment frequency are modelled as:

$$t_q = 1/f \qquad f = \sqrt{\frac{4}{3}\frac{g|\rho_v - \rho_l|}{\rho_l d_d}}, \tag{28}$$

The third heat flux density q_e used for evaporation is given by:

$$q_e = f\frac{\pi d_d^{\,3}}{6}\rho_v \ell n. \tag{29}$$

3.2.5 Wall function model for boiling flow

In order to take into account the influence of bubbles in the near wall area, a modified logarithmic law of the wall was suggested by Ramstorfer et al. (2005) and Koncar et al. (2008), which is usually used for turbulent flows over rough walls and reads

$$u^+ = \frac{1}{\kappa}\ln(y^+) + B - \Delta u^+ \tag{30}$$

where $u^+ = u_t / u_w$, $y^+ = \rho_l u_w \Delta y / \mu_l$ and $u_w = \sqrt{\tau_w / \rho_l}$ (τ_w is the wall shear stress). Here u_t is the known velocity tangential to the wall and Δy is the distance from the wall. Coefficients κ and B are standard single-phase constants with the values of 0.41 and 5.3, respectively. The last term represents the offset of u^+ due to the wall roughness

$$\Delta u^+ = \begin{cases} 0; & k_r^+ \le 11.3 \\ \frac{1}{\kappa}\ln(1 + C_{kr}k_r^+); & k_r^+ > 11.3 \end{cases} \tag{31}$$

(C_{kr}=0.5 for sand-grain roughness) and k_r^+ is the so-called roughness Reynolds number:

$$k_r^+ = \frac{\rho_l k_r \sqrt{u_w u^*}}{\mu_l}, \tag{32}$$

where $u^* = c_\mu^{\,1/4} k_l^{\,1/2}$ and $k_r = \alpha d$.

We have also tested $k_r^+ = \frac{\rho_l k_r u_w}{\mu_l}$ but results are not changed (figure 6).

4 EVM WEAKNESSES: THEORETICAL APPROACH.

Flows encountered in vertical pipe are of great interest to validate the most important heat, mass and momentum closure relations. However, some negligible effects in simple geometry sometimes become preponderant in complex geometries. For example, the modelling of two-phase flow in water cooled nuclear reactors needs to take into account swirls and stagnation points. Applications in complex geometries also need to take into account the complex features of the secondary motions which are observed experimentally. These requirements highlight the need for meticulous turbulence modelling.
A reason for the persistent widespread use of low level turbulence modelling in two-phase CFD is perhaps the fact that the use of two-phase CFD in complex industrial geometries is only starting. Moreover, many studies merely require “order of magnitude” or “good tendencies” answers.

However, extensive testing and application over the past three decades have revealed a number of

shortcomings and deficiencies in EVM models, and among them the $K-\varepsilon$ model, such as:

- Limitation to linear algebraic stress-strain relationship (poor performances wherever the stress transport is important, e.g.: non equilibrium, fast evolving, separating and buoyant flows);
- Insensitivity to the orientation of turbulence structure and stress anisotropy (poor performances where normal stresses play an important role, e.g.: stress-driven secondary flows in noncircular ducts);
- Inability to account for extra strain (streamline curvature, skewing, rotation);
- Poor prediction particularly of flows with strong adverse pressure gradients and in reattachment regions.

In a plane strain situation, such as upstream of a stagnation point on a bluff body, the exact (as obtained by a RTSM) production and that obtained from an EVM are respectively (Hanjalic, 2002):

$$P_{exact} = -(\overline{u_x'^2} - \overline{u_y'^2})\frac{\partial V_{l,x}}{\partial x} \text{ and } P_{EVM} = 4\nu_{l,t}(\frac{\partial V_{l,x}}{\partial x})^2 .$$

The difference between the normal stresses actually grows slowly on the short time scale needed for the flow to travel around the stagnation point, so the production remains moderate, and in any case is bounded, whereas P_{EVM} usually yields a severe over-prediction when the strain is high.

The simulation of swirling flow generated by the mixing vanes is our main goal since it plays an important role for the prediction of the CHF for the fuel assemblies. For this reason, the rotation effects are more specifically addressed hereafter.

It can be easily shown (Chassaing, 2000) that in the presence of an initially anisotropic turbulence, rotation will cause a redistribution of energy between normal components without affecting the value of this quantity. In fact, the angular velocity Θ does not appear explicitly in the K-equation, obtained by adding the normal stresses:

$$\frac{dK}{dt} = -\varepsilon$$

Thus, the $K-\varepsilon$ model is totally blind to rotation effects. The swirling flows can be regarded as a special case of fluid rotation with the axis usually aligned with the mean flow direction so that the Coriolis force is zero. This aspect is crucial for the simulation of hot channel of a fuel assembly. In fact, the mixing vanes of the spacer grids generate a swirl in the coolant water, to enhance the heat transfer from the rods to the coolants in the hot channels and to limit boiling.

In the following section, we present some examples of large-scale industrial applications, performed using eddy-viscosity models, and subsequently discuss areas of weakness of the models, highlighting some improvements that can be obtained through the use of more advanced stress transport closures.

5 ILLUSTRATION ON THE SINGLE-PHASE TEST AGATE-MIXING EXPERIMENT

Keeping in mind the long-term objective (two-phase CFD calculations validated under typical Pressurized Water Reactor (PWR) geometries and thermal-hydraulic conditions), we started very recently to evaluate NEPTUNE_CFD against spacer grid type experiments. An experimental device representing three mixing blades (figure 2) was introduced in a heated tube (diameter = 19.2 mm) and used for two different programmes:

- AGATE-mixing experiment (Falk, 2003): single-phase liquid water tests, with Laser-Doppler liquid velocity measurements upstream and downstream of mixing blades (for each of the 15 horizontal planes, the liquid velocity is measured along 12 different diameters and there are 12 points for each radius); the velocity at inlet is 3 m/s and the pressure is 2 bar.

- DEBORA-mixing experiment (Falk, 2002): boiling R12 refrigerant tests, on the same geometry but the total length of the calculation domain is 3.5 m; the tube is heated and the uniform wall heat flux is 109300 W/m^2 which generates about 2% of vapour at outlet; the outlet pressure is 26.2 bar; the inlet liquid temperature is 63.3 °C; the inlet liquid mass flow is 0.873 kg/s. The main physical phenomena to reproduce are: wall boiling, entrainment of bubbles in the wakes, and recondensation (Mimouni, 2008). So the prediction of the swirls is crucial.

For the mixing blades part (60 mm) 77000 cells are needed. The figure 1 compares computed and experimental azimuthal liquid velocity downstream of the mixing vane (AGATE test). One can notice the rotating flow is qualitatively well reproduced by NEPTUNE_CFD although the velocity is underestimated. This is mainly due to the turbulence model (standard $K-\varepsilon$ here) which is not optimum for this type of geometry.

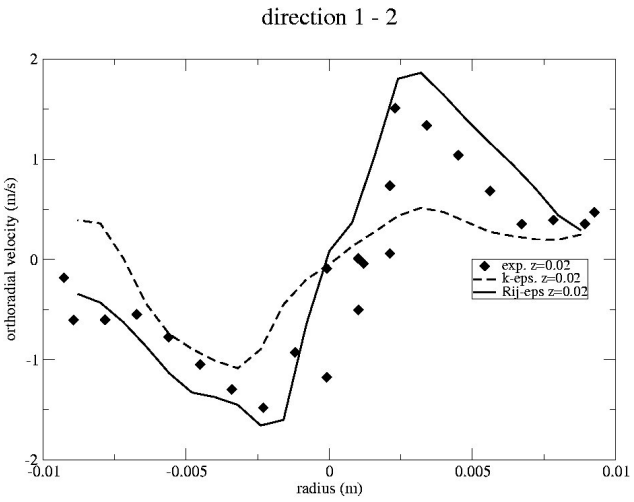

figure 1: Azimuthal liquid velocity downstream of the mixing vane (Agate-mixing experiment).

figure 2: View of the mixing device

The $K-\varepsilon$ model underestimates azimuthal velocities downstream of the blades but the results remain qualitatively satisfactory. The $R_{ij}-\varepsilon$ model gives satisfactory results (figure 1).

In the following section, we propose a second-moment closure model to take into account the liquid turbulence in order to validate, in the long-term, calculations in typical Pressurized Water Reactor (PWR) geometries and thermal-hydraulic conditions.

In the present paper, we suppose that RSTM is well-known in single phase flow (Hanjalic, 2002). Now, our objective is to test and if possible to improve our RSTM model adapted to bubbly flows as compared to experimental data and $K-\varepsilon$ results. Indeed, we are interested by two-phase high Reynolds numbers flows, but beforehand, the mechanical models implemented in the NEPTUNE_CFD code must be validated against boiling flows in analytical geometry.

6 THE SECOND-MOMENT CLOSURE MODEL FOR HIGH REYNOLDS NUMBER FLOWS DEDICATED TO THE CONTINUOUS PHASE (LIQUID).

In this section we omit the subscript “l” for the liquid and “α” is the void fraction for the sake of simplicity.

6.1 Equation on R ij

$$(1-\alpha)\frac{D\rho R_{ij}}{Dt} = \frac{\partial}{\partial x_k}\left\{\left(\rho\nu + \rho C_s \frac{K}{\varepsilon} R_{ij}\right)\frac{\partial}{\partial x_k}\left((1-\alpha)\cdot R_{ij}\right)\right\} + (1-\alpha)(P_{ij} + G_{ij} + \Phi_{ij} + \varepsilon_{ij}) \quad (33)$$

In this model, the Reynolds stress tensor of the continuous phase is split into two parts: a turbulent dissipative part produced by the gradient of mean velocity and by the wakes of the bubbles and a pseudo-turbulent non-dissipative part induced by the displacements of the bubbles. The displacements of the bubbles should be taken into account in experiments where air is injected at the bottom of a water pool creating a large, axi-symmetric bubble plume with a large-scale recirculation flow around the plume. But swirling flows and high Reynolds number characterize our industrial applications.

Hence, we neglected, in our approach and as a first analysis, the non-dissipative component called "pseudo-turbulent". We consider only the "turbulent" dissipative part. Within this framework, the term of production by the bubbles interfaces is written as (Chahed, 1999)

$$-\overline{(\frac{p}{\rho}u_i' n_j + \frac{p}{\rho}u_j' n_i)\delta^I + \nu(\frac{\partial}{\partial x_k}u_i' u_j')n_k\delta^I} \quad (34)$$

where n indicates the normal to the interface and δ^I a Dirac function on the interface. It was omitted in (Chahed, 1999). Indeed, according to (Chahed, 1999) dissipation in the wakes is balanced by the interfacial production: the equation of transport of the Reynolds stress tensor has the same form as in the single-phase case and is given by (10). When the void fraction is vanishing, the two-phase flow modelling naturally degenerates to the single-phase flow modelling.

Some terms of the equation of transport of the Reynolds stress tensor cannot be computed directly and must be modelled. A modelling resulting from (Hanjalic, 2002) is proposed below.
A common way to model the viscous destruction of stresses for high Reynolds number flows is:

$$\varepsilon_{ij} = \frac{2}{3}\varepsilon\delta_{ij} \quad (35)$$

The turbulent diffusion is of diffusive nature and the most popular model is the generalized gradient diffusion: $D_{ij}^t = \frac{\partial}{\partial x_k}\left(C_s \frac{K}{\varepsilon}\overline{u_k' u_l'}\frac{\partial \overline{u_i' u_j'}}{\partial x_l}\right)$ (36)

Pressure fluctuations tend to disrupt the turbulent structures and to redistribute the energy to make turbulence more isotropic: $\Phi_{ij} = \Phi_{ij,1} + \Phi_{ij,2} + \Phi_{ij,3} + \Phi_{ij,1}^{\omega} + \Phi_{ij,2}^{\omega}$, with:

- $\Phi_{ij,1} = -C_1\varepsilon\left(\frac{\overline{u_i' u_j'}}{K} - \frac{2}{3}\delta_{ij}\right)$ with $C_1 = 1.8$ (37)

- $\Phi_{ij,2} = -C_2\left(P_{ij} - \frac{2}{3}P\delta_{ij}\right)$ with $P = \frac{1}{2}P_{kk}$ and $C_2 = 0.6$
  $\Phi_{ij,3} = -C_3\left(G_{ij} - \frac{2}{3}G\delta_{ij}\right)$ $G = \frac{1}{2}G_{kk}$ $C_3 = 0.55$ (38)

- $\Phi_{ij,1}^{\omega} = C_1^{\omega}\frac{\varepsilon}{K}\left(\overline{u_k' u_m'}\underline{n_k}\underline{n_m}\delta_{ij} - \frac{3}{2}\overline{u_i' u_k'}\underline{n_k}\underline{n_j} - \frac{3}{2}\overline{u_k' u_j'}\underline{n_k}\underline{n_i}\right)\cdot f_{\omega}$ (39)

- $\Phi_{ij,2}^{\omega} = C_2^{\omega}\left(\Phi_{km,2}\underline{n_k}\,\underline{n_m}\delta_{ij} - \frac{3}{2}\Phi_{ik,2}\underline{n_k}\,\underline{n_j} - \frac{3}{2}\Phi_{jk,2}\underline{n_k}\,\underline{n_i}\right)\cdot f_{\omega}$ (40)

with: $C_1^{\omega} = 0.5 \quad C_2^{\omega} = 0.3 \quad f_{\omega} = \frac{0.4.K^{\frac{3}{2}}}{\varepsilon.x_n}$ where x $_n$ is the distance to the wall and $\underline{n_k}$ the base vector normal to the wall. The terms $\Phi_{ij,1}^{\omega}, \Phi_{ij,2}^{\omega}$ are implemented in the code but are not used in the calculations because they don't improve the results.

- *G* is the production by body force.

6.2 Equation on ε

In the RTSM closures the same basic form of model equation for ε is used as in the $K-\varepsilon$ model, except that now $\left(\overline{u_k' u_l'}\right)$ is available, which has the following implications:

- The production of kinetic energy (*P* and *G*) in the source term of ε are treated in exact form;
- The generalized gradient hypothesis is used to model turbulent diffusion.

Hence, the model equation for ε has the form:

$$(1-\alpha)\frac{D\varepsilon}{Dt} = \frac{\partial}{\partial x_k}\left(C_{\varepsilon}\frac{K}{\varepsilon}\overline{u_k' u_l'}\frac{\partial(1-\alpha)\varepsilon}{\partial x_l}\right) + \left(C_{\varepsilon_1}P + C_{\varepsilon_3}G + C_{\varepsilon_4}K\frac{\partial V_k}{\partial x_k} - C_{\varepsilon_2}\varepsilon\right)\cdot\frac{(1-\alpha)\varepsilon}{K} \qquad (41)$$

The coefficients of the $R_{ij}-\varepsilon$ model are:

C_s	C_1	C_2	C_1^{ω}	C_2^{ω}	C_{ε}	C_{ε_1}	C_{ε_2}	C_{ε_3}	C_{ε_4}
0.2	1.8	0.6	0.5	0.3	0.18	1.44	1.92	1.44	0.33

Table 1: coefficients of the $R_{ij}-\varepsilon$ model

7 DEBORA CASE

7.1 Brief description of the DEBORA experiment

The tests were performed on the DEBORA loop at CEA-Grenoble with R12 refrigerant as a cooling fluid (Manon, 2000). Global flow data are given in Table 2. The calculation domain is a vertical cylindrical tube of 19.2 mm internal diameter and 3.485 m heated length. At the measuring station (end of the heated length), we compare numerical results against experimental data for the axial vapour velocity, the void fraction and the liquid temperature.

P_s (outlet pressure) (MPa)	flowrate G (kg/m²s)	Heat Flux (kW/m^2)	T_e (liquid temperature at inlet) (°C)	X_s (outlet quality)
2.62	1996	73893	68.52	0.058
Table 2: global flow data of the DEBORA test 29G2P26W16Te68_1				

The bubble diameter is equal to 0.3 mm in accordance with experimental observations.

7.2 Simulations of the DEBORA experiment

The flow is assumed to be axisymmetric therefore a two-dimensional axisymmetric meshing is used. Computations have been performed on three kinds of meshing with the $R_{ij}-\varepsilon$ turbulence model and the wall function model dedicated to boiling flows and proposed in the paper: a coarse grid (20 cells in the radial direction and 100 cells in the axial direction), a medium grid (20 cells in the radial direction and 200 cells in the axial direction) and a fine grid (30 cells in the radial direction and 200 cells in the axial direction). Results are similar (figure 3), hence the subsequent calculations were performed on the first grid. A difference on the liquid temperature is observed, but its magnitude is small.

The void fraction profile illustrates that vapour bubbles are nucleated onto the heated wall surface and condense in the subcooled liquid in the core of the flow. The liquid temperature profile is the combination of several phenomena: the liquid near the wall is heated by the single phase flow convective heat flux q_c plus the quenching heat flux q_q; bubbles condense in the subcooled liquid in the core of the flow and heat the liquid; the molecular and turbulent heat fluxes inside the liquid phase modify the temperature profile. The liquid turbulent heat flux depends on the values of K_l and ε and therefore depends on the turbulence modelling: on the figure 4, the $R_{ij}-\varepsilon$ model gives better results than the $K-\varepsilon$ model which means that $K-\varepsilon$ model over-estimates the liquid turbulent heat flux.

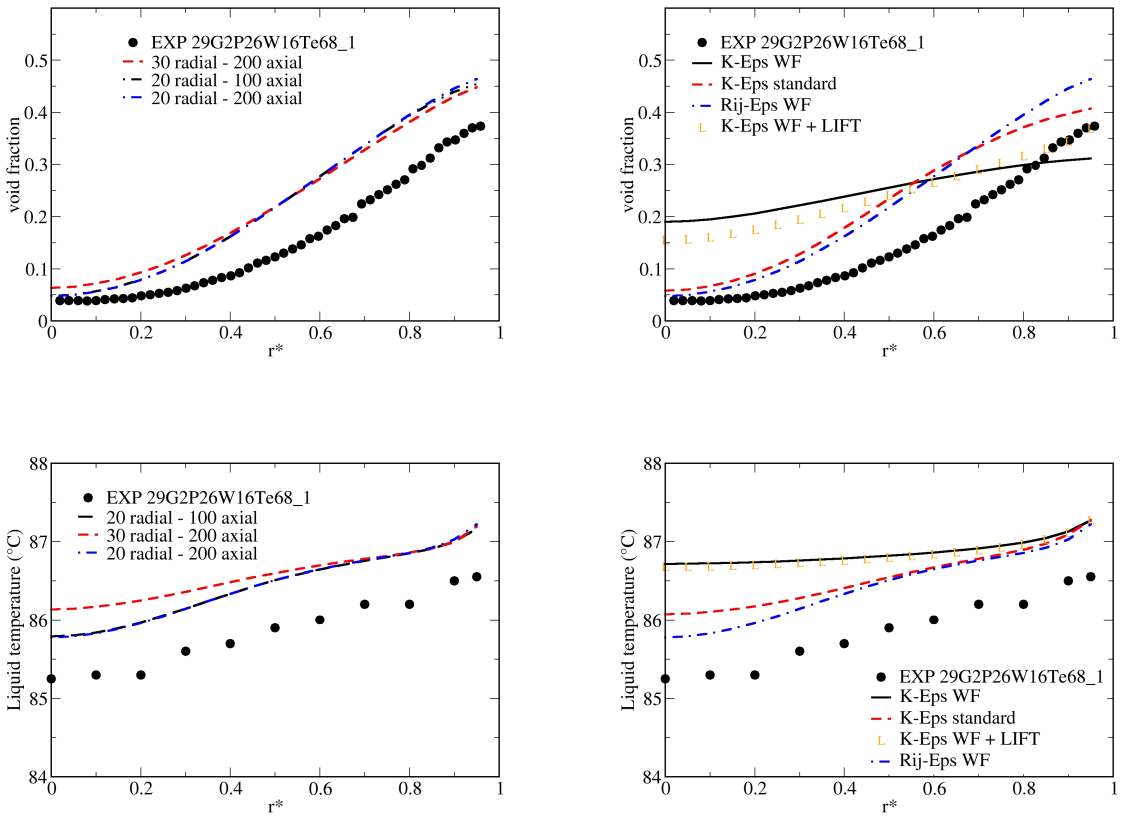

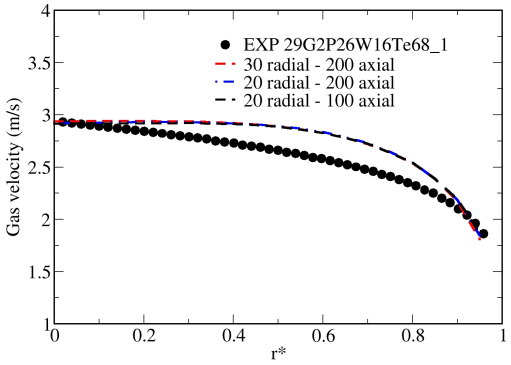

figure 3: Sensitivity to the mesh refinement

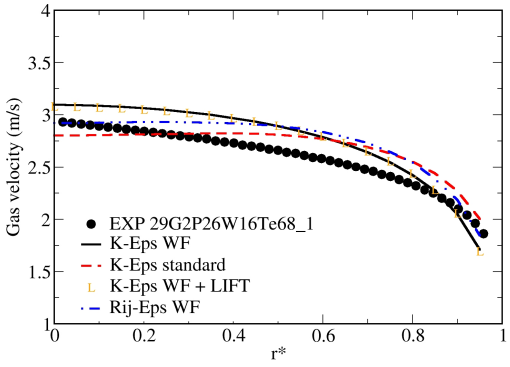

figure 4: Sensitivity to the lift force and to the wall function (WF) model.

On the figure 4, we study the effect of the lift force on the void fraction, liquid temperature and axial vapour velocity calculated with the $K-\varepsilon$ turbulence model for the liquid phase. Calculations with lift force ("K-eps WF + LIFT") and without lift force ("K-eps WF") give similar results. Great values of the liquid mass flow rate and bubbles diameter of order of 0.3 mm make the bubbles follow the liquid stream lines. The relative velocity is weak and so, the lift force is small. As a consequence, the lift force is neglected, which is a desirable simplification since it may cause numerical instabilities when used in conjunction with the $R_{ij}-\varepsilon$ turbulence model. We only consider the drag, added-mass and turbulent dispersion force in the following computations.

Following Koncar et al (2008), wall function model have been implemented to take into account the modification of the single phase logarithmic wall law for boiling cases. When using the $K-\varepsilon$ turbulence model, the void fraction is overestimated in the core with the wall function model (WF). Without this model, the results of the standard wall function (standard) model are in quite good agreement with the experimental data.

Computations with the $R_{ij}-\varepsilon$ model used in conjunction with the WF model give globally a quite good agreement with the experimental data even if they slightly overestimate the void fraction near the wall.

8 ASU CASE

8.1 Brief description of the ASU experiment

The Arizona State University (ASU) experiment is described in (Hasan, 1990) and (Roy, 1993) for two-phase boiling flow measurements. The test section of the ASU experiment consists of a vertical annular channel with a heated inner wall and an insulated outer wall. The inner tube is made of 304 stainless steel (i.d. = 14.6 mm, o.d. = 15.9 mm) and the outer pipe of transparent pyrex glass (inlet diameter = 38.1 mm, outlet diameter = 47 mm) except for a 0.496 m long measurement section which is made of quartz (i.d. = 37.7 mm, o.d. = 41.7 mm). The inner tube is resistively heated, the upper 2.75 m of the 3.66 m long test section being the heated length. The lower 0.91 m serves as the hydrodynamic entrance length. The working fluid is refrigerant 113 (R113).

When the inner wall heating is sufficiently high, heterogeneous nucleation appears onto this wall surface. As the inlet liquid is subcooled, the bubbles condense into the colder liquid when they are far from the inner wall layer. According to Roy et al. (Roy, 1993), a two layer is observed: a boiling bubbly layer adjacent to the heated wall and an outer all liquid region. A dual-sensor optical fibre probe and a

microthermocouple were installed diametrically opposite each other in the measurement section. The measurement plane was approximately located at 1.94 m downstream of the beginning of the heated length. The dual-sensor optical fibre probe was used to measure the radial profiles of the different quantities characterizing the dispersed phase (void fraction, bubble axial velocity and bubble chord length). The bubble chord length distribution allows to compute the bubble diameter distribution, hence the local interfacial area concentration, by making several assumptions (see (Roy,1993) for more explanations). However, these authors conclude that further work is needed before the local interfacial area concentration can be determined with confidence.

The bubble diameter is equal to 1.2 mm in the calculations in accordance with experimental observations.

We have the radial profiles of the void fraction, the mean axial liquid velocity, the mean liquid temperature and the radial fluctuations of the liquid velocity for two different experimental cases we name TP5 and TP6. The controlling parameters for these cases are indicated in table 3 below.

Case	Pressure, bar	Wall heat flux, W/m^2	Inlet mass flow rate, kg/m^2s	Inlet temperature, °C
tp5	2.69	95	784	50.2
tp6	2.69	116	784	50.2

Table 3: Experimental conditions retained for our simulations.

8.2 Simulations of the ASU experiment

For the experimenters, the advantage of using an annular geometry instead of a pipe is that the flow field can be studied by intrusive probes (e.g. optical fibre probes, microthermocouples) or non intrusive probes (e.g. Laser Doppler Velocimeter) without having to disrupt the heated wall (Roy, 1993). For us, the advantage of this particular geometry is to test the validity of our models for a boiling flow around a *convex* heated wall instead of inside a *concave* one as it is the case for a simple pipe. This change of wall convexity can have some important effects on the flow evolution. In a general manner, it is advantageous to test the models we have retained for boiling flows on different experiments characterized by different working fluids (R113 for ASU / R12 for DEBORA), different wall heatings, different inlet liquid flow rates and subcoolings…

The length of the ASU calculation domain is equal to 3.30 m and the last 2.39 m length are heated. The flow is assumed to be axisymmetric therefore a two-dimensional axisymmetric calculation grid has been used. Computations have been performed on three kinds of meshing with the RTSM turbulence model and the wall function model: a coarse grid (20 cells in the radial direction and 100 cells in the axial direction), a medium grid (30 cells in the radial direction and 100 cells in the axial direction) and a fine grid (20 cells in the radial direction and 200 cells in the axial direction). Results are similar. Hence, the subsequent computations were performed on the first grid (figure 5).

Following Koncar (Koncar, 2008) and the conclusions of the previous test case (namely the DEBORA test), the forces acting on the bubbles that were retained are the drag, added-mass and turbulent dispersion forces.

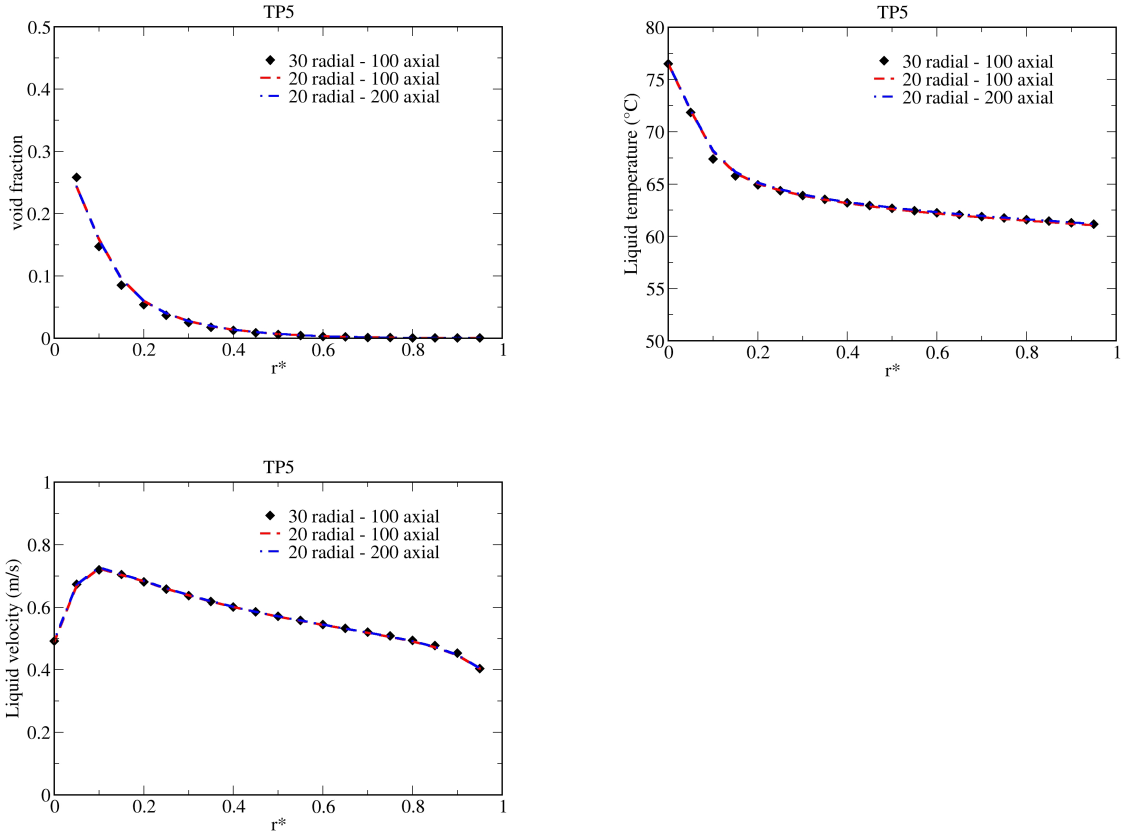

figure 5: Sensitivity to the mesh refinement (RSTM+WF).

The liquid velocity profile calculated with the $K-\varepsilon$ model is improved when using the WF model. We think that the discrepancy observed on the liquid mean axial velocity may be due to a bad estimation of the liquid axial velocity near the heated wall. This would not be surprising since we use the classical *single-phase* logarithmic velocity profile to express the boundary condition on the liquid velocity (wall friction law).

Void fraction and liquid temperature profiles are similar with or without the WF model. Moreover, all the profiles computed the RSTM model are practically unchanged with the WF model (figure 6). So, the WF model is adopted by default in the subsequent computations ($K-\varepsilon$ and $R_{ij}-\varepsilon$).

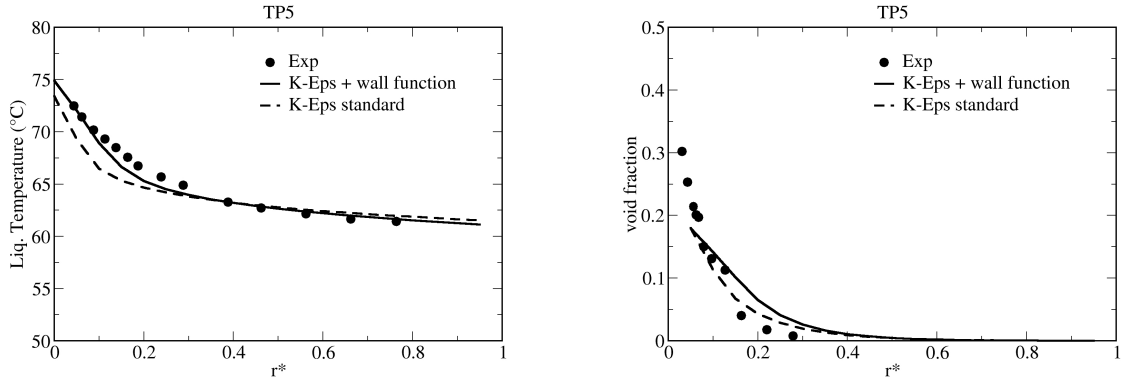

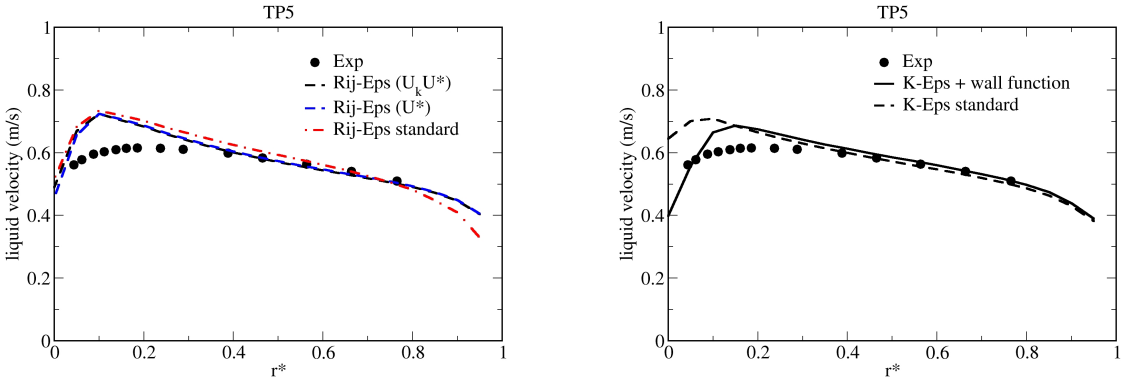

figure 6: Sensitivity to the wall function (WF) model.

We compare the RSTM and $K-\varepsilon$ models for the void fraction (figure 7), the liquid temperature (figure 8), the liquid axial velocity (figure 9), the liquid turbulent kinetic energy (figure 10) and the radial fluctuations of the liquid velocity (figure 11). The liquid temperature profiles are in quite good agreement with the experimental data with both turbulence models.

The local void fraction at a given point is the result of the competition between several physical phenomena like bubble nucleation and condensation, bubble lateral migration, bubble relative axial velocity… Liquid temperature and axial liquid velocity profiles are similar with both turbulence models but the void fraction profile is particularly well predicted with the RSTM model. In fact, radial fluctuations of the liquid velocity give satisfactory results near the wall where most of the bubbles are concentrated. For the $K-\varepsilon$ model, radial and axial velocity fluctuations are the same.

Particularly near the wall, we observe a quite good agreement between the calculations using the RSTM model and the experimental data (see the void fraction for the TP5 and TP6 tests on the figure 7), which is crucial for the prediction of the boiling crisis in PWR conditions.

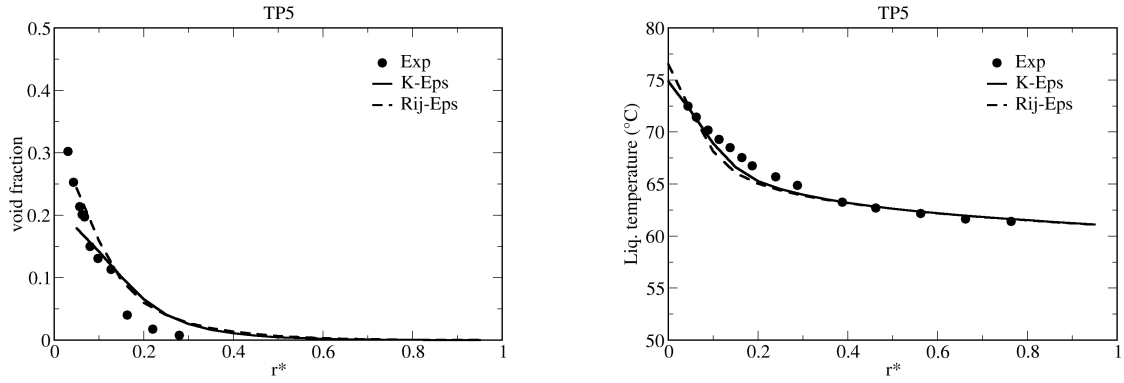

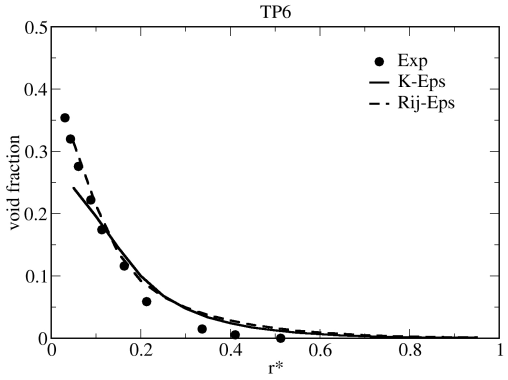

figure 7: Void fraction with the WF model.

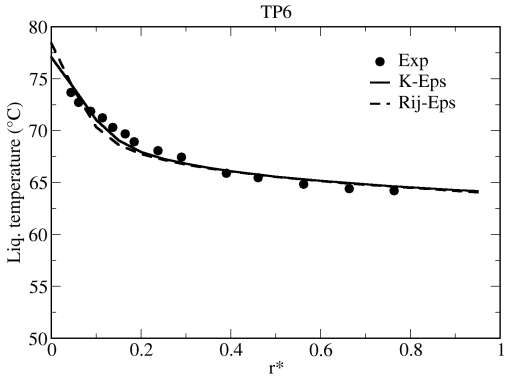

figure 8: Liquid temperature with the WF model.

The liquid turbulent kinetic energy are slightly more correctly predicted near the wall with the RSTM model but calculations using the $K-\varepsilon$ model give slightly more satisfactory results in the core of the flow (figure 10). The radial fluctuations of the liquid velocity give better results with the RSTM model (figure 11).

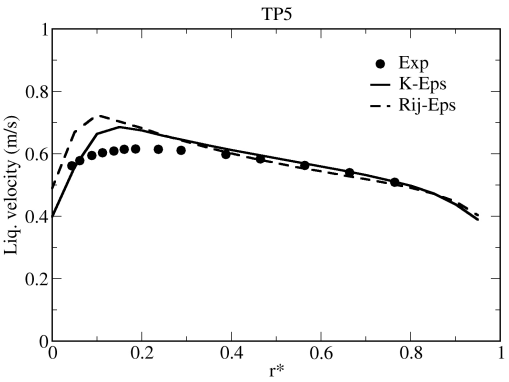

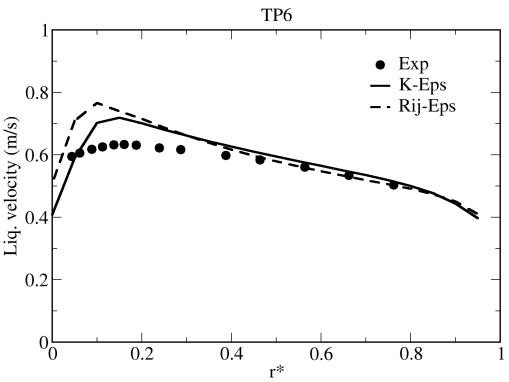

figure 9: Liquid velocity with the WF model.

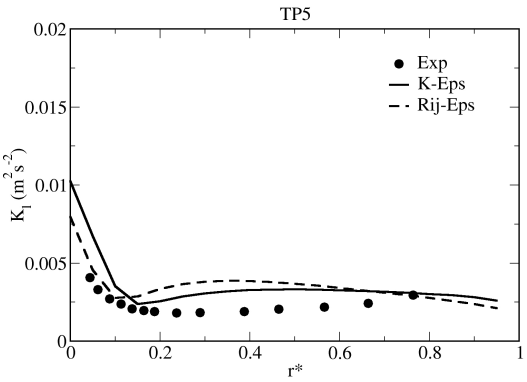

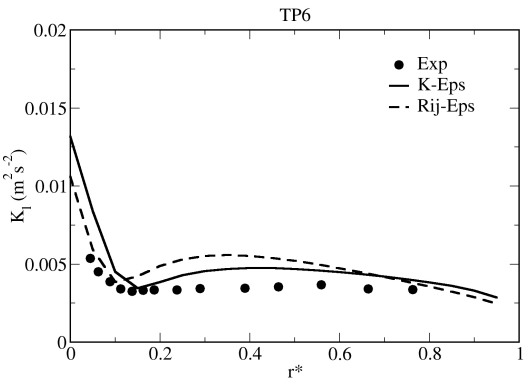

figure 10: Liquid turbulent kinetic energy (WF).

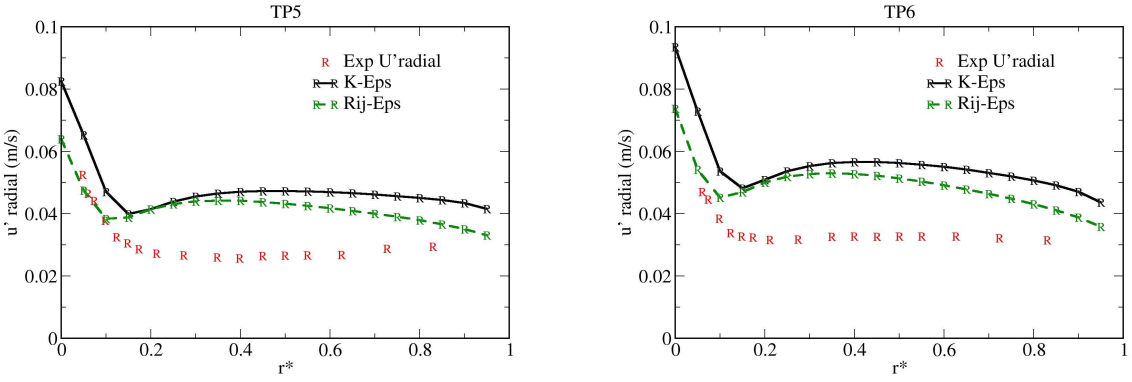

figure 11: Radial fluctuations of the liquid velocity (WF).

Even in this analytical geometry, where the turbulent intensities calculated by both turbulence models are relatively weak, we observe a difference on variables like the void fraction or the liquid velocity.

9 CALCULATIONS OF A 2X2 ROD BUNDLE

A geometry closer to actual fuel assemblies is considered (Shin, 2002). It consists of a rectangular test section in which a 2x2 rod bundle equipped with a simple spacer grid with mixing vanes (figure 12-figure 13-figure 15). The geometry of the mixing vanes is different from (Shin, 2002) and so we don't have experimental data but the calculations performed in this section will allow estimating our current capabilities to simulate boiling flows with a RSTM with a geometry closer to actual fuel assemblies.

The thermal-hydraulics conditions are representative of PWR core configurations close to nominal. At inlet, the liquid temperature is 603K and the axial velocity is 5m/s. The outlet pressure is 155 bar.

An adiabatic single-phase liquid velocity profile establishes in the 0.3 m inlet section. Above this limit, a uniform heat flux is imposed along the rods up to 0.9 m upstream of the mixing vanes. This heat flux is equal to 1.6MW so that the void fraction reaches a maximum value of about 70%.
Following Koncar (Koncar, 2008) and the conclusions of DEBORA test, the forces acting on the bubbles that are retained are the drag and the added-mass forces. The turbulent dispersion is taken into account by the Tchen's theory.

Calculations have been performed with three kinds of meshing with the RTSM turbulence model and the $K-\varepsilon$ turbulence model: a coarse grid (figure 16), a medium grid (figure 17) and a fine grid (figure 18).
The mean axial liquid velocity (profile 1 and 2) upstream of mixing blades are presented figure 19 and figure 20. Results are similar and do not depend on the grid refinement. But for the profile 1, the $K-\varepsilon$ model on the finest mesh give slightly higher values because the mesh near the wall is much too fine and then the usual logarithmic law is replaced by a condition of vanishing velocity at the wall. Therefore, in order to conserve the mass flowrate, the liquid velocity takes higher values in the core of the flow.
The height Z=0 mm corresponds to the beginning of the spacer grid. The mean azimuthal liquid velocity (profile 1) just above the mixing blades at the height Z=40mm is illustrated on figure 21. Results are similar and do not depend on the grid refinement. Downstream of the mixing blades, at Z=200mm, the mean azimuthal velocity (profile 1) predicted using the $K-\varepsilon$ model is much lower than that predicted with the $R_{ij}-\varepsilon$, as expected from the theory. This fact is also clear on figure 25, figure 26, figure 27 and figure 28. Therefore, the mixing of the flow predicted with the $K-\varepsilon$ model is smaller than with the $R_{ij}-\varepsilon$ model.

The liquid temperature in the flow is the combination of several phenomena as already discussed in the DEBORA test. The turbulent heat flux is directly proportional to $\nu_l^T = C_\mu \frac{K_l^2}{\varepsilon_l}$ and the $K-\varepsilon$ usually yields a severe over-prediction of K_l downstream of the mixing blades. The $K-\varepsilon$ model under estimates the mixing but over-predicts the turbulent coefficient diffusion of heat flux. The liquid temperature fields for both turbulence models are presented figure 23 and figure 24: the liquid temperature calculated with the $K-\varepsilon$ model is more homogeneous in the calculation domain, i.e. the gradient of temperature is lower. As a consequence, the void fraction fields downstream of the mixing blades have slightly lower values with the $K-\varepsilon$ model than the $R_{ij}-\varepsilon$ model. A second order closure for the turbulent heat flux should be used in future calculations to take into account the anisotropy of the turbulent heat fluxes, which is needed to detect hot points on the rod surface in the frame of the boiling crisis.

The time step is about 10^{-5} s to ensure a CFL equal to 1. As for the computational costs, the results are synthesized in the table 4. The RSTM over-cost is about 36% for single-phase flow but reaches 56% for boiling flow.

The over-cost with the $R_{ij}-\varepsilon$ model for boiling flows is important but remains reasonable when using a super-computer with 64 processors.

	Single-phase flow	Boiling flow
$K-\varepsilon$; coarse grid	3,0 s	3,3 s
$K-\varepsilon$; medium grid	6,5 s	9,9 s
$K-\varepsilon$; fine grid	20,1 s	25,5 s
$R_{ij}-\varepsilon$; fine grid	27,5 s	40,0 s

Table 4: CPU time by time step.

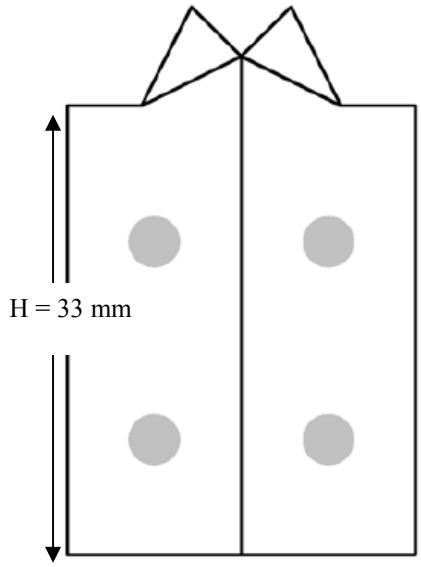

figure 12: spacer grid with mixing vanes

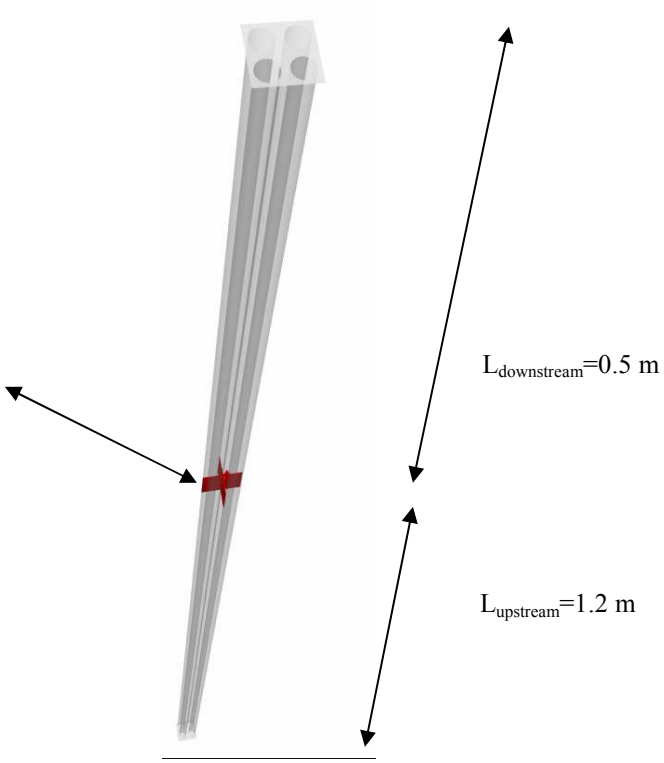

figure 13: 2x2 rod bundles.

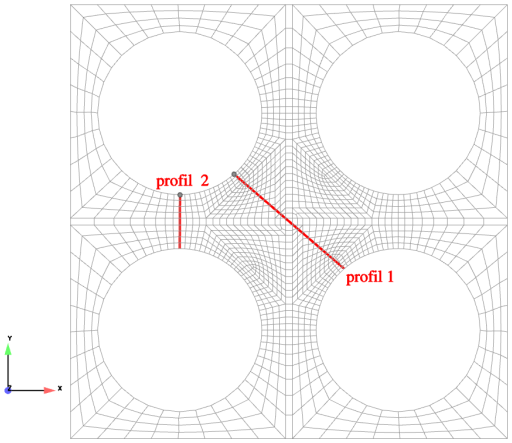

figure 14: liquid velocities are calculated along profiles 1 and 2.

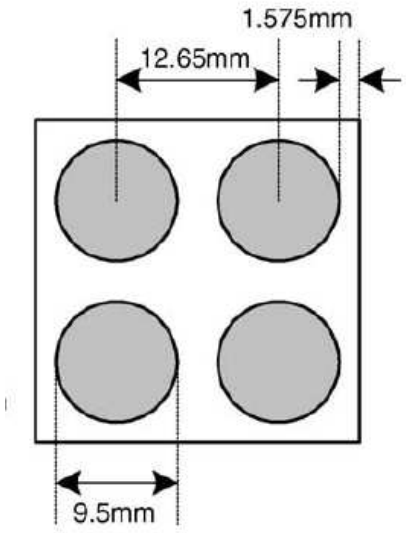

figure 15: 2x2 rod bundles (Shin, 2002).

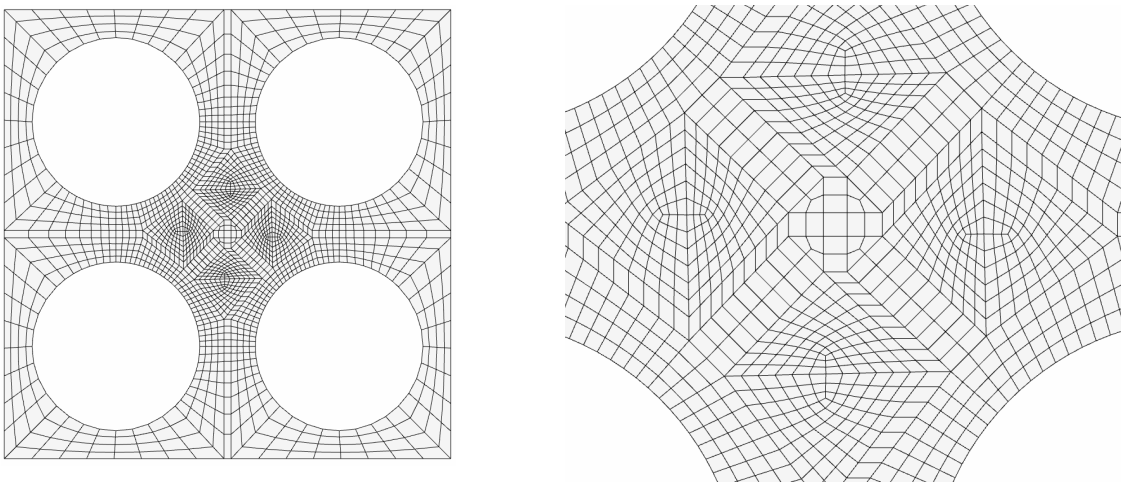

figure 16: Coarse meshing : 1 651 508 cells (zoom at right).

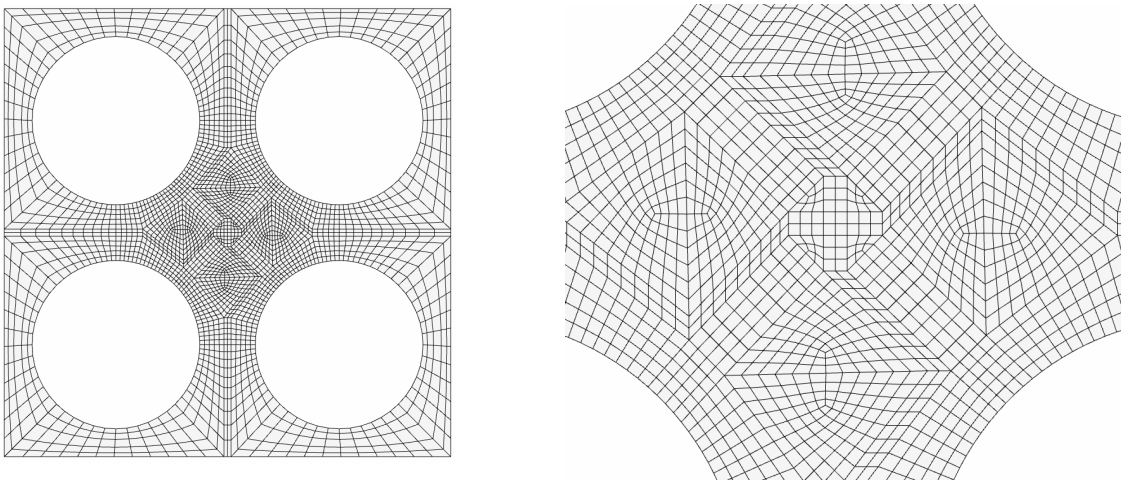

figure 17: Medium meshing : 3 366 976 cells (zoom at right).

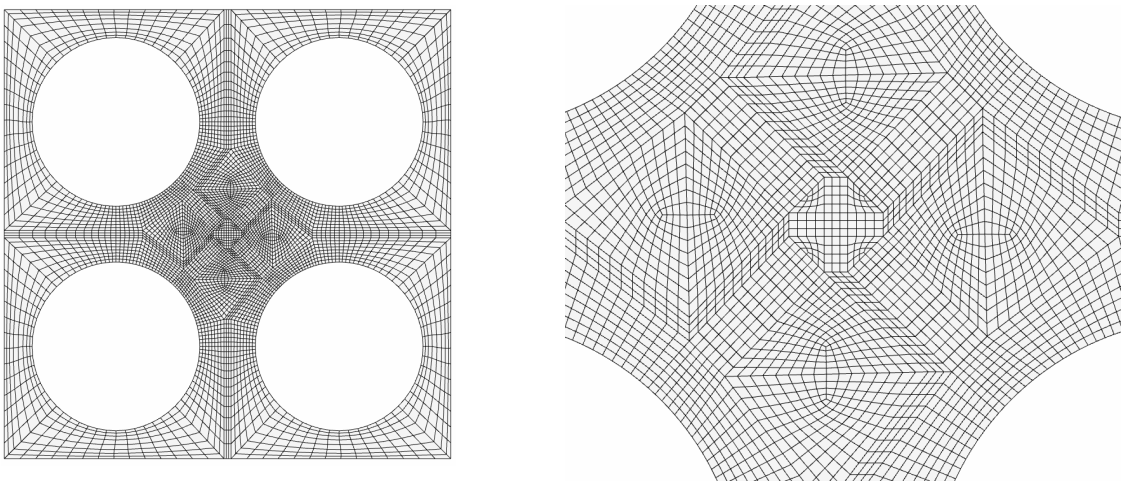

figure 18: Finest meshing : 7 629 583 cells (zoom at right).

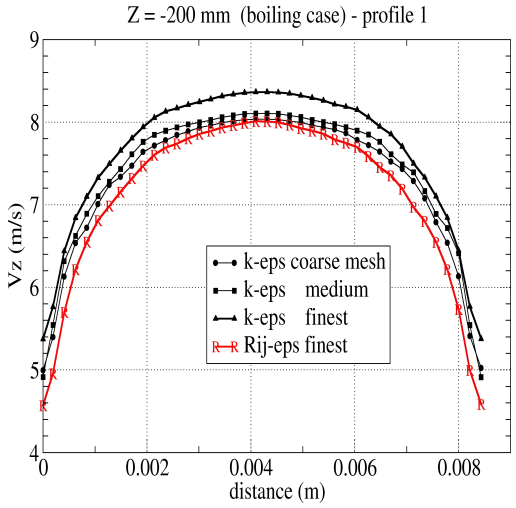

figure 19: mean axial liquid velocity (profile 1) upstream of mixing blades.

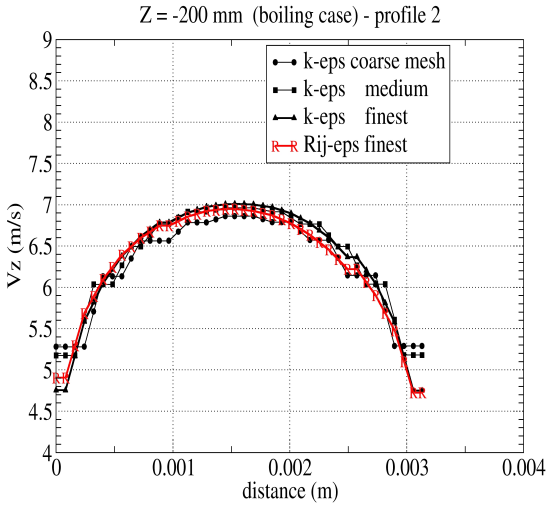

figure 20: mean axial liquid velocity (profile 2) upstream of the mixing blades.

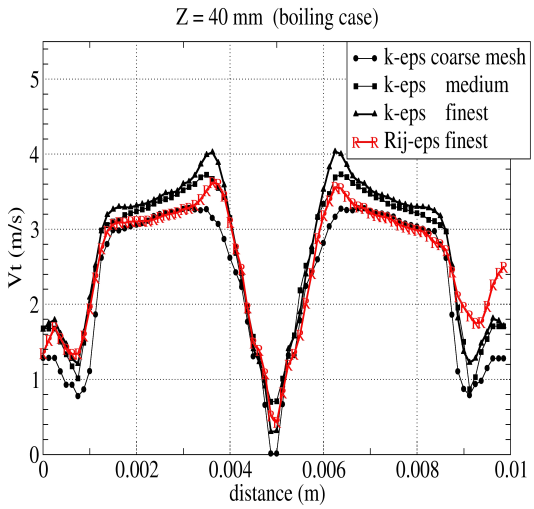

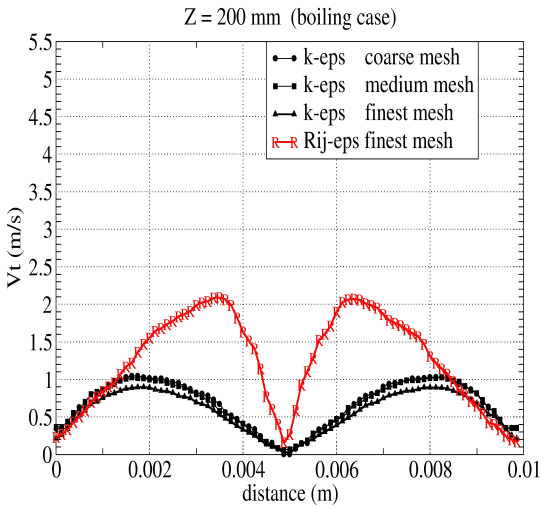

figure 21: mean azimuthal liquid velocity (profile 1) just above the mixing blades.

figure 22: mean azimuthal liquid velocity (profile 1) downstream of the mixing blades.

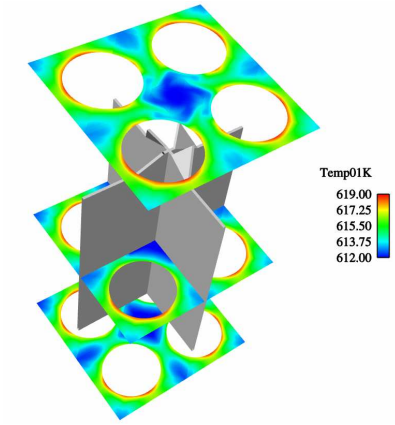

figure 23: liquid temperature ($K-\varepsilon$).

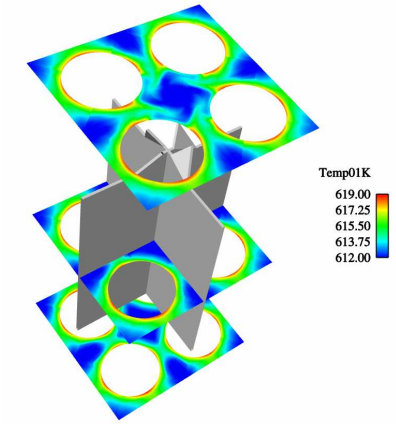

figure 24: liquid temperature ($R_{ij}-\varepsilon$)

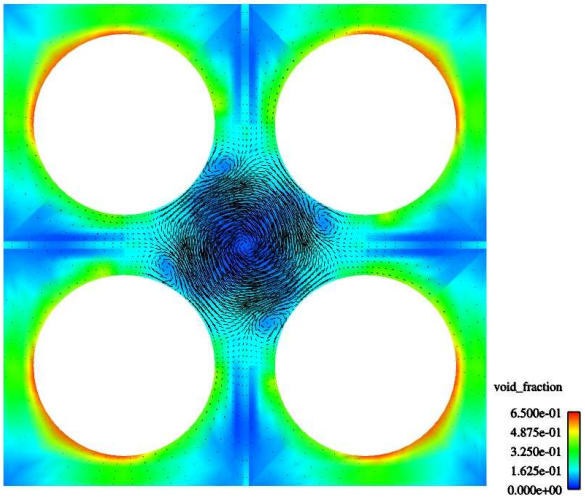

figure 25: void fraction just above the mixing blades at Z=40 mm ($K-\varepsilon$).

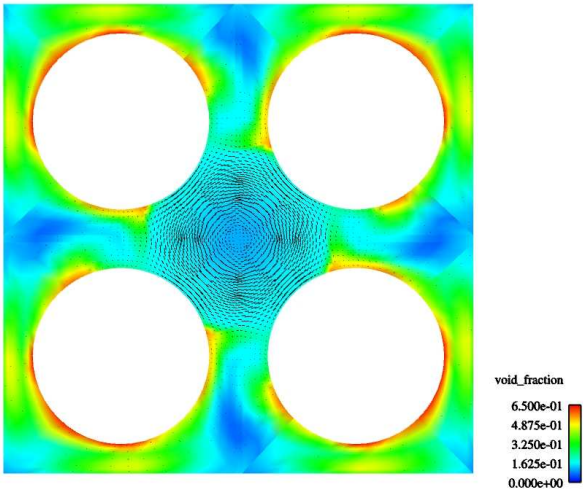

figure 26: void fraction downstream of mixing blades at Z=200 mm ($K-\varepsilon$).

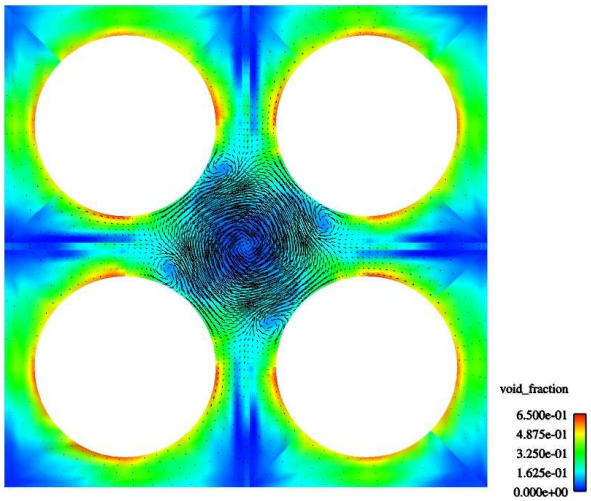

figure 27: void fraction just above the mixing blades at Z=40 mm ($R_{ij}-\varepsilon$)

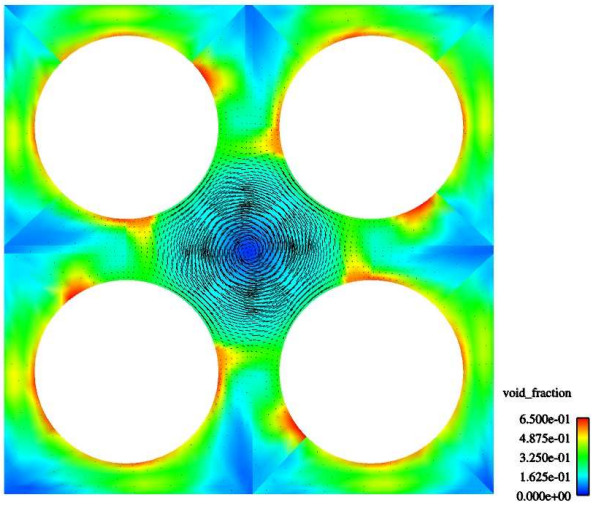

figure 28: void fraction downstream of mixing blades at Z=200 mm ($R_{ij}-\varepsilon$).

10 CONCLUSION AND PERSPECTIVES

An analysis of turbulence modelling for two-phase flows in fuel assemblies has been proposed. Indeed, the use of eddy viscosity models is widespread and may be sufficient for parallel flows in vertical pipes, but that type of model does not account for effects that are preponderant in complex geometries, especially when swirling flows are involved, for example in pressurized water reactor cores downstream of mixing vanes and spacer grids. In accordance with the theory, it is shown in the case of a flow downstream of a mixing vane that using a Reynolds Stress model is an efficient way to improve the simulation of such complex flows. To demonstrate that the use of a Reynolds Stress model is not bound to deteriorate the classical results obtained with an eddy viscosity model, a validation step on more analytical experiments has been carried out in (Mimouni, 2008b) (bubbly flows in a straight pipe and in a sudden expansion): the study shows that the Reynolds Stress Model implemented in the multiphase 3D code NEPTUNE_CFD satisfactorily reproduces the results obtained with the standard eddy viscosity model and both compare reasonably well with the experiments in such configurations. This first conclusion has been extended to the two-phase boiling flows in the present paper.

Calculations in a geometry closer to actual fuel assemblies in PWR thermal-hydraulics conditions show that the $K-\varepsilon$ and $R_{ij}-\varepsilon$ models may predict globally the same void fraction level because of errors compensations with the $K-\varepsilon$ model downstream of mixing vanes.

As the void fraction is directly related to the liquid temperature field, a second order closure for the turbulent heat flux should be used in future calculations.

As for the computational cost, we note that in the case of the 2x2 rod bundle test that the RSTM over-cost is about 36% for single-phase flow but reaches 56% for boiling flow.

Moreover, amongst the developments planned in the medium term, we have identified the need for a polydispersion model allowing a local prediction of the bubble size distribution.

Besides, it may be indicated that the NEPTUNE project has set up a medium and long term experimental programme to acquire detailed measurements in simplified and real geometries, both in adiabatic and real conditions (Guelfi, 2007).

11 ACKNOWLEDGEMENTS

This work has been achieved in the framework of the NEPTUNE project, financially supported by CEA (Commissariat à l'Énergie Atomique), EDF (Électricité de France), IRSN (Institut de Radioprotection et de Sûreté Nucléaire) and AREVA-NP.

12 REFERENCES

S.P. Antal, R.T. Lahey Jr, J.E. Flaherty, "Analysis of phase distribution in fully developped laminar bubbly two-phase flow", *International Journal of Multiphase Flow*, vol. 17, No 5, pp. 635-652 (1991).

T.R. Auton, "The lift force on a spherical body in a rotational flow", *J. Fluid Mech.*, Vol. 183, pp. 199-218 (1987).

R. Bel Fdhila, "Analyse expérimentale et modélisation d'un écoulement vertical à bulles dans un élargissement brusque", *PhD Thesis*, Institut National Polytechnique de Toulouse. In French, 1991.

D. Bestion, D., "synthesis of work performed in WP2.2", *6th Euratom Framework Program NURESIM,* deliverable D2.2.1.1b ((2007).

J. Chahed, "Forces interfaciales et turbulence dans les écoulements à bulles: Modélisation et étude de cas de référence", *PhD Thesis,* l'université des sciences et techniques de Tunis. In French, 1999.

P. Chassaing, *Turbulence en mécanique des fluides*, éditions Cépaduès. In French, 2000.

C.P. Cheung, G.H. Sherman, G.H. Yeoh, J.Y. Tu, “On the numerical study of isothermal vertical bubbly flow using two population balance approaches”, *Chemical Engineering Science* 62 4659 – 4674 (2007).

J-M. Delhaye, M. Giot, and M.L. Riethmuller, M. L., *Thermal-hydraulics of two-phase systems for industrial design and nuclear engineering*. Hemisphere and McGraw Hill, 1981.

E. Deutsch, O. Simonin, “Large eddy simulation applied to the motion of particles in stationary homogeneous fluid turbulence”, *in Turbulence Modification in Multiphase Flows, ASME FED*, vol. 110, 1991, pp. 35–42.

F. Falk, A. Giacommelli, A., “Rapport d’essais AGATE PROMOTEUR DE MELANGE”, *technical report* CEA DTP/SETEX/LTAC/03-191. Internal report in French, 2003.

F. Falk, R. Hugonnard, “Rapport d’essais DEBORA PROMOTEUR DE MELANGE, essais de BO et de topologie, campagne 4800-4900-5000”, *technical report* , CEA DTP/SETEX/LTAC/02-158. Internal report in French, 2002.

A. Guelfi, D. Bestion, M. Boucker, P. Boudier, P. Fillion, M. Grandotto, J-M. Hérard, E. Hervieu, P. Péturaud, “NEPTUNE - A new software platform for advanced nuclear thermal hydraulics”, *Nuclear Science and Engineering*, vol. 156, pp. 281-324, 2007.

Hanjalic and D. Laurence, *Introduction to Turbulence Modelling*, Lecture series 2002-02, March 18/22, 2002.

A. Hasan, R.P. Roy, S.P. Kalra, “Experiments on subcooled flow boiling heat transfer in a vertical annular channel”, *International Journal of Heat and Mass Transfer*, Volume 33, Issue 10, Pages 2285-2293 (1990).

K. Ikeda, Y. Makino, M. Hoshi, “Single-phase CFD applicability for estimating fluid hot-spot locations in a 5x5 fuel rod bundle”, *Nuclear Engineering and Design* 236 (2006) 1149-1154.

W.K. In, T-H. Chun, C-H. Shin, “Numerical computation of heat transfer enhancement of a PWR rod bundle with mixing vane spacers”, *Nuclear Technology* vol. 161 JAN. 2008.

M. Ishii M., *Thermo-fluid dynamic, theory of two phase*, Eyrolles, collection de la direction des Etudes et recherches d’Electricité de France, 1975.

M. Ishii; *Two-fluid model for two-phase flow*, Multiphase Science and Technology, Hewitt G.F., Delhaye J.M., Zuber N. Eds., Vol. 5, pp. 1-58 (1990).

B. Končar, E. Krepper, “CFD simulation of convective flow boiling of refrigerant in a vertical annulus”, *Nuclear Engineering and Design*, Volume 238, Issue 3, Pages 693-706 (2008).

E. Krepper, B. Koncar, Y. Egorov, “CFD modelling of subcooled boiling – Concept, validation and application to fuel assembly design”, *Nuclear Engineering and Design* 237 716-731 (2007).

Kurul and M.Z. Podowski, “Multidimensional effects in forced convection subcooled boiling”, *Proceedings of the Ninth International Heat Transfer Conference* Jerusalem, Israel, August (1990), pp. 21–26 (1990).

M. Lance, M. Lopez de Bertodano, *Phase distribution phenomena and wall effects in bubbly two-phase flows*, Multiphase Science and Technology, Vol. 8, Hewitt G.F., Kim J.H., Lahey R.T. Jr., Delhaye J.M. & Zuber N., Eds, Begell House, pp. 69-123 (1994).

C.M. Lee, Y.D. Choi, “Comparison of thermo-hydraulic performances of large scale vortex flow (LSVF) and small scale vortex flow (SSVF) mixing vanes in 17x17 nuclear rod bundle”, *Nuclear Engineering and Design* 237 (2007) 2322-2331

E. Manon, "Contribution à l’analyse et à la modélisation locale des écoulements bouillants sous-saturés dans les conditions des Réacteurs à Eau sous Pression", *PhD thesis*, Ecole Centrale Paris, 2000.

S. Mimouni, A. Archer, J. Laviéville, M. Boucker, N. Méchitoua, « Modeling and computation of unsteady cavitation flows”, *La Houille Blanche*, N°6, 2006.

S. Mimouni, M. Boucker, J. Laviéville, A. Guelfi, D. Bestion, “Modeling and computation of cavitation

and boiling bubbly flows with the NEPTUNE_CFD code", *Nucl. Eng. And Design* 238 (2008) pp 680-692.

S. Mimouni, F. Archambeau, M. Boucker, J. Laviéville, C. Morel, "A second order turbulence model based on a Reynolds stress approach for two-phase flow – Part I : adiabatic cases", *Science and Technology For Nuclear Installations*, in press, 2008(b).

B. Ramstorfer, H. Breitschadel, G. Steiner, "Modelling of the near-wall liquid velocity field in subcooled boiling flow", *Proceedings of the ASME Summer Heat Transfer Conference* San Francisco, CA, July (2005) HT2005-72182 (2005).

R.P. Roy, V. Velidandla, S.P. Kalra, P. Péturaud, "Local measurements in the two-phase boiling region of turbulent subcooled boiling flow", *ASME Journal of Heat Transfer*, 1993.

B.S. Shin, S.H. Chang, "Experimental study on the effect of angles and positions of mixing vanes on CHF in a 2x2 rod bundle with working fluid R-134a", *Nuclear Engineering and Design* 235 pp 1749-1759 (2005).

A. Tomiyama, A., "Struggle with computational bubble dynamics", *3rd Int. Conf. Multiphase Flow ICMF'98*, Lyon, France, June 8-12 (1998).

A. Tomiyama, K. Sakoda, G.P. Celata, I. Zun, "A simple method for evaluating fluctuating bubble velocity and its application to a hybrid bubble tracking method", *3rd Int. Symposium on Two-Phase Flow Modeling and Experimentation*, Pisa, Italy, September 22-24 (2004).

H.C. Unal, "Void fraction and incipient point of boiling during the subcooled nucleate flow boiling of water", *International Journal of Heat and Mass Transfer* 20 (1977), 409-419.

Zhou, Yang, Lian, Fan & Lee, "On the second-order moment turbulence model for simulating a bubble column", *Chemical Engineering Science* 57, pp 3269 – 3281 (2002).

N. Zuber, „On the dispersed two-phase flow in the laminar flow regime", *Chem. Eng. Sc*., No. 19, p. 897 (1964).